Renewable Energy 143 (2019) 679–691

Contents lists available at ScienceDirect

Renewable Energy

journal homepage: www.elsevier.com/locate/renene

A semi-analytical noise prediction model for airfoils with serrated trailing edges

Yannick D. Mayer [a], Benshuai Lyu [b], Hasan Kamliya Jawahar [a], Mahdi Azarpeyvand [a, *]

[a] Faculty of Engineering, University of Bristol, Bristol, BS8 1TR, United Kingdom
[b] Department of Applied Mathematics and Theoretical Physics, University of Cambridge, Cambridge, CB3 0WA, United Kingdom

ARTICLE INFO

Article history:
Received 22 February 2019
Received in revised form
11 April 2019
Accepted 24 April 2019
Available online 6 May 2019

Keywords:
Aeroacoustics
Trailing edge serrations
Scattering
Boundary layer
Trailing edge noise

ABSTRACT

Trailing edge serrations are a widely used passive technique for the suppression of aerodynamic noise from wind turbines. Despite their popularity, no reliable engineering prediction tool has yet been developed to estimate the noise reduction for different serrations. This paper concerns the development of an engineering noise prediction tool, based on a recently developed mathematical model. Results show that the new model has several advantages over Howe's model, as it can take both destructive and constructive sound interference effects into account. Two surface pressure wavenumber-frequency models are implemented, namely Chase and TNO models, to demonstrate the sensitivity of the model to boundary layer characteristics. The boundary layer parameters needed in the wavenumber-frequency models are obtained using RANS CFD simulations. Far-field noise comparisons are provided between the proposed prediction tool and experimental data for a NACA0018 airfoil. A parametric study regarding the boundary layer changes of serrated airfoils signifies the need for more reliable wavenumber-frequency models. The results presented in the paper show that the proposed engineering tool can provide a fairly accurate estimate of the noise reduction performance of serrated airfoils, but its accuracy relies heavily on the availability of reliable near-field boundary layer information.

1. Introduction

The rapid expansion and the rising prevalence of wind turbines have resulted in negative, noise associated, health effects for a large number of people living in the vicinity of airports or large wind farms [1]. The European Union, amongst other governmental bodies worldwide, has introduced more stringent regulations to limit these adverse effects. Hence, it is now a key requirement and a critical design driver to reduce the aerodynamic noise from wind turbines in order to comply with the existing and future noise regulations. A study by Venugopal et al. [2] in the context of wind turbines reasoned that for a given maximum overall sound pressure level, a noise reduction of 1 dBA allows a larger blade to be utilized and the annual harvested energy to be increased by 2–3%, revealing the economic and practical importance of reducing aerodynamic self-noise from wind-turbines.

It is generally recognized that out of the five different airfoil self-noise mechanisms identified by Brooks [3], the dominant aerodynamic noise source for attached flows is the turbulent boundary layer trailing edge noise. Trailing edge noise is generated when turbulent flow structures pass the trailing edge and are subsequently scattered at the edge [4]. In order to reduce the trailing edge noise, various treatments, such as serrations, riblets and porous material have been investigated [4–7]. The use of serrations represents a passive and cost-effective solution to mitigate the sound radiated from airfoils, by introducing destructive interference between the scattered sound fields. A multitude of serration geometries have been investigated experimentally. After initially focusing on sinusoidal and sawtooth serrations, more recently, novel serrations such as slitted, slitted-sawtooth and sawtooth-sinusoidal serrations [8] as well as concave serrations [9,10] were examined in order to further increase the noise reduction capabilities of the serration technology. Several experimental studies by Dassen et al. [11], Moreau et al. [12], Gruber [13] and Leon et al. [14], Oerlemans et al. [15] among others have also examined the sound reduction potential of serrated trailing edges, while Liu et al. [16] and Chong et al. [17] have investigated the aerodynamic changes

* Corresponding author. Queen's Building, BS8 1TR, Bristol, United Kingdom.
E-mail addresses: yannick.mayer@bristol.ac.uk (Y.D. Mayer), bl362@cam.ac.uk (B. Lyu), hasan.kj@bristol.ac.uk (H.K. Jawahar), m.azarpeyvand@bristol.ac.uk (M. Azarpeyvand).

https://doi.org/10.1016/j.renene.2019.04.132
0960-1481/

due to the presence of serrations. Recently, Ragni et al. [18], Sanders et al. [19] and Avallone et al. [20,21] have investigated the effect of serrations on the hydrodynamic near-field and found a low-frequency reduction of the surface pressure spectra towards the serration tip, as well as an increase of the spanwise correlation length.

Current trailing edge noise prediction methods include numerical, semi-empirical and analytical methods. Computational aeroacoustics (CAA) approaches either simultaneously calculate the hydrodynamic and acoustic fields, i.e. direct numerical simulations (DNS) [22], or use high-quality flow simulations as input into acoustic noise propagation models [23–27], such as the Ffowcs Williams and Hawkings model [28], which takes monopole, dipole and quadrupole noise sources into account. A common approach is to use Large Eddy Simulation to achieve relatively high Reynolds numbers in combination with the Ffowcs Williams and Hawkings propagation model, which has been used for a variety of applications [29–31]. The CAA approaches are often used only for better understanding of the physics of noise generation and rarely used for industrial design purposes due to the high computational cost. Alternatively, semi-empirical methods can be employed, such as the popular BPM model [3], however, their accuracy is questionable when flow parameters or geometry deviate from those in the underlying investigation. With regards to analytical models, Amiet for example proposed a model which simplifies the airfoil as a flat plate. The scattered pressure on the surface of the plate is deduced, and in order to calculate the far-field noise, the Kirchhoff radiation integral is evaluated [32]. This model was later extended by Roger and Moreau [33] to take the leading-edge back-scattering effects into account, which improves the predictions at low-frequencies. Modeling the underlying physics more accurately was the aim of other analytical models, such as the TNO model [34], which have reduced the reliance on semi-empirical models and their intrinsic limitations. Recent improvements include the coupling of the TNO model to RANS simulations or panel methods, as for example proposed by Bertagnolio et al. [35].

Whilst the prediction capabilities for trailing edge noise are steadily moving toward maturity, the noise reduction from serrated trailing edges has been a challenging problem. Howe proposed a model which was able to demonstrate that sawtooth serrations provide substantial noise reduction [4]. However, it was reported that the model overpredicts the noise reduction greatly [36]. Following a similar approach to Howe, Azarpeyvand et al. [8] extended this model to slitted, slitted-sawtooth and sawtooth-sinusoidal serrations. Recently, Lyu et al. [37] developed a serrated trailing edge model based on Amiet's theory of trailing edge noise using an iterative procedure, and the solution has been validated against the results from a finite element simulation. The predicted noise reduction results for sawtooth serrations were found to be more realistic compared to experimental results. This is believed to be due to the fact that the iterative solution proposed in Ref. [37] provides a more accurate modeling to the scattering response than the Green's function used by Howe. The first-order solution of the Lyu et al. model has recently been implemented by Fischer et al. [38] to predict the sound reduction of serrated airfoils. More recently, Huang [39] proposed a theoretical model to solve the acoustic scattering problem for arbitrary but periodically serrated trailing edges, by applying the Fourier expansion and Wiener-Hopf method. He also confirmed the criteria developed by Lyu et al. with regards to effective noise reduction using serrated trailing edges. Another very recent model was proposed by Ayton [40], where the Wiener-Hopf method was also used to obtain the far-field sound power spectral density for a semi-infinite flat plate with arbitrary but periodic trailing edge serrations.

This paper implements the full second order-solution of Lyu et al. [37] and combines it with both the TNO and Chase wavenumber-frequency ($\mathbf{k}-\omega$) spectra to predict the far-field noise. Firstly, the model developed by Lyu et al. as well as the model developed by Howe will be reintroduced and compared briefly in Section 2. Section 2 will present a validation of the model by Lyu et al. against the Amiet solution for a straight trailing edge. Section 3 will then detail the implementation of the different wavenumber-frequency spectra, namely the Chase model and TNO model. Subsequently, the noise-reduction prediction for a NACA 0018 airfoil with a serrated trailing edge is presented in Section 4 and compared to experimental data found in the literature. The required flow field inputs are taken from a CFD simulation which is also detailed in Section 4. Lastly, the concluding remarks and future work are outlined in Section 5.

2. Serration model overview

This section will firstly reintroduce the scattering model developed by Lyu et al. for airfoils with serrated trailing edges and will demonstrate its consistency with Amiet's model. Hereafter, the scattering model from Lyu et al. will be referred to as STE model for brevity. Secondly, Howe's model will be presented and discussed briefly as a comparison to the STE model.

2.1. Serrated trailing edge noise model (STE)

The airfoil under consideration is modelled as a flat plate, as illustrated in Fig. 1, where c denotes the average chord and d the span. The serration amplitude is $2h$ and the serration wavelength is denoted by λ. x', y' and z' denote the streamwise, spanwise and normal-to-plate coordinates with the far-field observer located at $\mathbf{x} = x_1, x_2, x_3$, corresponding to a polar angle of θ and an azimuthal angle of ϕ. In order to calculate the scattered pressure field from the trailing edge, an oncoming gust of the form

$$p_i = P_i \mathrm{e}^{-\mathrm{i}(\omega t - k_1 x' - k_2 y')}, \tag{1}$$

is considered, as shown in Fig. 1. Here, P_i is the magnitude of the incident wall pressure gust with a frequency of ω and k_1 and k_2 represent the chordwise and spanwise wavenumbers, respectively. In what follows, the wavenumber vector will be denoted $\mathbf{k} = (k_1, k_2, k_3)$. As detailed by Amiet, the incident pressure gust causes a scattered field starting at the trailing edge due to the change in

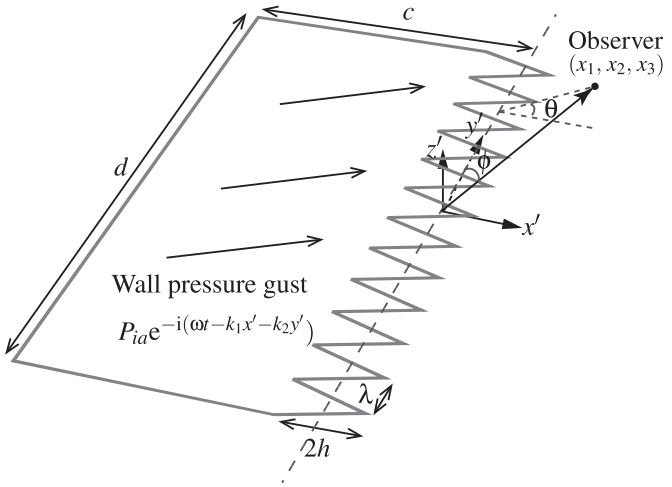

Fig. 1. Schematic of the idealized flat plate with trailing edge serrations, reproduced from Ref. [37].

boundary condition at the trailing edge [41]. The total pressure, p_t, consists of two parts, firstly, the incident pressure, p_i, and secondly, the scattered pressure, p_s, which neutralizes the incident pressure and thereby satisfies the Kutta condition of zero pressure gradient at the trailing edge. The wave equation governing the scattered pressure field has to be solved

$$\nabla^2 p_s - \frac{1}{c_0^2}\left(\frac{\partial}{\partial t} + U_\infty \frac{\partial}{\partial x\prime}\right)^2 p_s = 0, \tag{2}$$

where c_0 represents the speed of sound, U_∞ is the ambient mean flow velocity, and $M_0 = U/c_0$ is the mean flow Mach number. In the case of a serration with a geometric profile of $H(y')$, applying a coordinate transformation, $x = x' - H(y')$, $y = y'$, $z = z'$, and assuming harmonic perturbations, $p_s = P(x', y', z')\mathrm{e}^{-\mathrm{i}\omega t}$, Lyu et al. derived the following partial differential equations

$$\begin{aligned}&\left(\beta^2 + H'^2(y)\right)\frac{\partial^2 P}{\partial x^2} + \frac{\partial^2 P}{\partial y^2} + \frac{\partial^2 P}{\partial z^2} - 2H'(y)\frac{\partial^2 P}{\partial x \partial y}\\ &+ \left(2\mathrm{i}M_0 k_0 - H''(y)\right)\frac{\partial P}{\partial x} + k_0^2 P = 0,\end{aligned} \tag{3}$$

where $k_0 = \omega/c_0$ and $\beta^2 = 1 - M_0^2$. $H'(y)$ and $H''(y)$ denote the first and second derivative of the serration profile, respectively [37]. A Fourier expansion of the form

$$P(x, y, z) = \sum_{-\infty}^{\infty} P_n(x, z)\mathrm{e}^{\mathrm{i}k_{2n}y} \tag{4}$$

can be applied due to the periodicity of the scattering in the spanwise direction, to obtain the following equation

$$\begin{aligned}&\left\{\left(\beta^2 + H'^2(y)\right)\frac{\partial^2}{\partial x^2} + \frac{\partial^2}{\partial y^2} + \frac{\partial^2}{\partial z^2} - 2H'(y)\frac{\partial^2}{\partial x \partial y}\right.\\ &\left.+ \left(2\mathrm{i}M_0 k_0 - H''(y)\right)\frac{\partial}{\partial x} + k_0^2\right\} \times \sum_{-\infty}^{\infty} P_n(x, z)\mathrm{e}^{\mathrm{i}k_{2n}y} = 0,\end{aligned} \tag{5}$$

where $k_{2n} = k_2 + 2n\pi/\lambda$. The summation $\sum_{-\infty}^{\infty} P_n(x, z)\mathrm{e}^{\mathrm{i}k_{2n}y}$ adds up the different modes of the scattered pressure. Substituting the sawtooth serration geometry and taking care of the singularities at the tip and root of each sawtooth, one can show that the following set of differential equations results

$$D\boldsymbol{P} - A\boldsymbol{P} = B\frac{\partial \boldsymbol{P}}{\partial x}, \tag{6}$$

where A and B are defined as follows

$$A_{ml} = \left(k_{2m}^2 - k_0^2\right)\delta_{ml}, B_{ml} = \begin{cases}\dfrac{4\sigma}{\lambda}\dfrac{m + l + k_2\lambda/\pi}{l - m}, & m - l \text{ is odd}\\ 0, & m - l \text{ is even},\end{cases} \tag{7}$$

with δ_{ml} representing the Kronecker delta. D is a differential operator and $P(x, z)$ is a vector of the different mode functions, given by

$$\mathrm{D} = \left\{\left(\beta^2 + \sigma^2\right)\frac{\partial^2}{\partial x^2} + \frac{\partial^2}{\partial z^2} + 2\mathrm{i}k_0 M_0 \frac{\partial}{\partial x}\right\}, \tag{8}$$

$$\boldsymbol{P} = \left(\cdots P_{-n'}(x, z),\ P_{-n'+1}(x, z),\ \cdots P_{n'-1}(x, z),\ P_{n'}(x, z),\ \cdots\right)^T. \tag{9}$$

A solution for P is derived using an iterative technique and solving the Schwarzschild problem at each iteration step. The details of the iterative technique can be found in Lyu et al. [37]. The scattered surface pressure field is obtained by adding up all different modes of $P_{n'}(x, 0)$ and transforming the solution back to the original coordinate system, that is

$$P(x', y', 0) = \sum_{n'=-\infty}^{\infty} P_{n'}(x' - H(y'), 0)\mathrm{e}^{\mathrm{i}k_{2n'}y'}, \tag{10}$$

where

$$\boldsymbol{P}(x, 0) = \boldsymbol{N}(x) + \boldsymbol{C}^{(1)}(x) + \boldsymbol{C}^{(2)}(x) + \boldsymbol{C}^{(3)}(x) + \cdots. \tag{11}$$

Finally, the far-field power spectral density, S_{pp}, is found in analogy to Amiet's model by applying a surface integral over k_2 to yield the far-field power spectral density in the midplane, $y' = 0$, of the idealized flat plate, namely

$$\begin{aligned}S_{pp}(\mathbf{x}, \omega) = &\left(\frac{\omega x_3 c}{4\pi c_0 S_0^2}\right)^2 2\pi d\\ &\times \sum_{m=-\infty}^{\infty} |\mathscr{L}\left(\omega, \overline{k_1}, 2m\pi/\lambda\right)|^2 \Pi(\omega, 2m\pi/\lambda)\end{aligned} \tag{12}$$

here, $\Pi(\omega, 2m\pi/\lambda)$ is the wavenumber-frequency, $\mathbf{k} - \omega$, spectrum integrated over k_1, $S_0^2 = x_1^2 + \beta^2(x_2^2 + x_3^2)$, $\overline{k_1} = \omega/U_c$ and U_c is the average convection velocity. The far-field sound gust-response function $\mathscr{L}$ is calculated iteratively in a similar way to the scattered surface pressure field as

$$\begin{aligned}\mathscr{L}(\omega, k_1, k_2) = &(1 - \mathrm{i})\frac{1}{\lambda c}\mathrm{e}^{-\mathrm{i}k_0(M_0 x_1 - S_0)/\beta^2}\mathrm{e}^{\mathrm{i}k_0(M_0 - x_1/S_0)h/\beta^2}\\ &\times \sum_{n'=-\infty}^{\infty}\left(\Theta_{n'} + \Theta_{n'}^{(1)} + \Theta_{n'}^{(2)} + \cdots\right).\end{aligned} \tag{13}$$

The complete mathematical formulation of each individual Θ term can be found in Lyu et al. [37]. Equation (12) also marks the underlying result of the STE model and reduces to Amiet's model when h/λ approaches zero, *i.e.* the serrated edge reduces to a straight edge. However, it has to be noted that whilst it is possible to have a point-spectrum as input into Amiet's model, this is not the case for the serrated trailing edge model which requires a wavenumber-frequency spectrum as input in order to calculate the sound reduction achieved with serrated trailing edges.

In order to validate that the STE model reduces to Amiet's trailing edge noise model for a straight trailing edge, experimental point spectra and the corresponding Amiet far-field noise predictions from Gruber [42] were used. Gruber conducted a large number of noise tests in varying flow conditions and the chosen test cases concern a NACA 0012 and a NACA 65(12)-10 airfoil with a chord length of 0.15 m and span of 0.45 m. The NACA 0012 airfoil was tested for $U_\infty = 40$ m/s at an angle of attack (AoA) of $\alpha = 0°$ and the NACA 65(12)-10 airfoil was tested for $U_\infty = 20$ m/s at $\alpha = 5°$. The airfoils were tripped at 10% of the chord on both the suction and pressure sides to achieve a fully turbulent boundary layer before the trailing edge. Gruber approximated the wavenumber-frequency spectrum, integrated over k_1 and k_2, as

$$\Pi(\omega) \approx G_{pp}(\omega) * l_y(\omega), \tag{14}$$

where $l_y(\omega) = \frac{b_c U_c}{\omega}$ and b_c is the Corcos constant, as adopted in Ref. [42]. The required surface pressure fluctuation point spectra near the trailing edge of the airfoil were extracted from the relevant surface pressure spectra plots provided in Ref. [42]. In order to

simulate the straight trailing edge with the STE model, the serration amplitude was set to approximately zero and the serration wavelength was assigned a very large value. Finally, the sound pressure level (*SPL*) is calculated as follows,

$$SPL(\omega) = 10\log_{10}\left(\frac{S_{pp}(\omega)}{p_0^2}\right), \tag{15}$$

where $p_0 = 20\mu$Pa.

Fig. 2 shows Gruber's far-field noise data measured at a location right above the trailing edge at a distance of $r = 1.2$ m and Gruber's Amiet noise predictions, as depicted in Ref. [42]. The figure also displays the noise predictions obtained from the STE model, Eq. (12), presented in this paper. It can be seen that for both validation test cases, the STE model matches Gruber's Amiet model very well. It is believed that the main reason for the small discrepancies is inaccurate data extraction from the figures presented by Gruber in Ref. [42], both for Gruber's Amiet prediction as well as for the surface pressure spectrum required in the $\mathbf{k}-\omega$ spectrum approximation. Based on the results in Fig. 2, it can be confirmed that the STE model implemented in this paper reduces to Amiet's model for straight trailing edges. More validations against FEM results can be found in Ref. [37]. It is very important to note though that the wavenumber-frequency spectrum approximation used here, *i.e.* surface pressure point spectrum multiplied by the spanwise correlation length, cannot be used for the prediction of the far-field noise reduction in the case of serrated trailing edges. This is the case because a surface pressure wavenumber-frequency spectrum is required as an input in Eq. (12), as opposed to a point spectrum approximation in Amiet's model.

2.2. Howe's trailing edge model

In order to provide a comprehensive study, Howe's trailing edge noise model is provided here, which will be used in the following sections for comparison against the STE model. According to Howe, the power spectral density of the far-field noise of a flat plate with a sawtooth trailing edge can be found from Ref. [43].

$$\frac{S_{pp}(\mathbf{x},\omega)}{(\rho_0 v_*)^2 (d/c_0)(\delta/|\mathbf{x}|)^2} = \frac{C_m}{\pi}\sin^2\left(\frac{\theta}{2}\right)\sin(\phi)\Psi(\omega), \tag{16}$$

where the non-dimensional edge noise spectrum $\Psi(\omega)$ is given by

$$\Psi(\omega) = \left(1+\frac{1}{2}\chi\frac{\partial}{\partial\chi}\right) f\left(\frac{\omega\delta}{U_c}, \frac{h}{\lambda}, \frac{h}{\delta}; \chi\right), \tag{17}$$

and

where ρ_0 is the density of air and δ is the boundary layer thickness. Howe's model uses Chase's $\mathbf{k}-\omega$ spectrum and hence, $C_m = 0.1553, \chi = 1.33$ and $v_* = 0.03U$. One can easily show that in the case of a flat plate without trailing edge serration, the non-dimensional edge noise spectrum reduces to

$$f\left(\frac{\omega\delta}{U_c}, \frac{h}{\lambda}, \frac{h}{\delta}; \chi\right) = \frac{1}{\left(\frac{\omega\delta}{U_c}\right)^2\left(1+\left(4\frac{h}{\lambda}\right)^2\right)+\chi^2} \times$$
$$\left(1+\frac{64\left(\frac{h}{\lambda}\right)^3\left(\frac{\delta}{h}\right)\left(\frac{\omega\delta}{U_c}\right)^2\left(\cosh\left(\left(\frac{\lambda}{2\delta}\right)\sqrt{\left(\frac{\omega\delta}{U_c}\right)^2+\chi^2}\right)-\cos(2\omega h/U_c)\right)}{\sqrt{\left(\frac{\omega\delta}{U_c}\right)^2+\chi^2}\left(\left(\frac{\omega\delta}{U_c}\right)^2\left(1+\left(4\frac{h}{\lambda}\right)^2\right)+\chi^2\right)\sinh\left(\left(\frac{\lambda}{2\delta}\right)\sqrt{\left(\frac{\omega\delta}{U_c}\right)^2+\chi^2}\right)}\right), \tag{18}$$

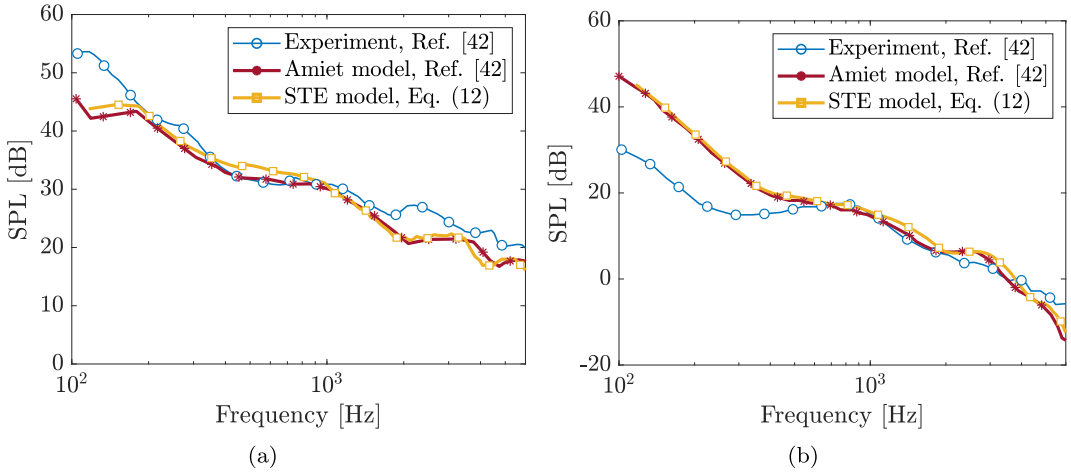

Fig. 2. Comparison of the STE model prediction with experimental data and Amiet's noise prediction from Gruber [42] for 0.15 m chord airfoils with a straight trailing edge: (a) NACA 0012 $U_\infty = 40$ m/s at $\alpha = 0$, (b) NACA 65(12)-10 $U_\infty = 20$ m/s at $\alpha = 5°$.

$$\Psi(\omega) = \frac{(\omega\delta/U_c)^2}{\left[(\omega\delta/U_c)^2 + \chi^2\right]^2}. \tag{19}$$

As a preliminary comparison between the STE and Howe's model, a parametric study of varying λ/h was performed. The parametric study was carried out for a plate with a serration length of $h/c = 0.2$, at a free stream velocity of $U_\infty = 30$ m/s and a boundary layer thickness of $\delta/c = 0.035$. The Chase wavenumber-frequency model [4] has been used as input to both the Howe and STE far-field noise models, termed STE-Chase and Howe-Chase, as shown in Fig. 3. Fig. 3 shows the reduction of the sound pressure level (ΔSPL), i.e. the effect of a serrated compared to a straight trailing edge case, for five different serration wavelengths, namely $\lambda/h = 0.125, 0.25, 0.5, 1.0, 2.0$. A positive ΔSPL is indicative of a far-field noise reduction. It can be seen that with decreasing λ/h, *i.e.* sharper serrations, both far-field noise models predict higher levels of noise reduction, with Howe's model consistently predicting greater noise reduction at high-frequencies. One interesting observation is that according to Howe's model (Fig. 3a) higher levels of noise reduction are achieved by using very sharp serrations (*i.e.* small λ/h), while the STE results in Fig. 3b reveal that after a certain λ/h, the use of even sharper serrations will only lead to further noise reduction at high-frequencies, with no noise benefit at lower frequencies. A similar behavior was also observed in the experimental results by Gruber [42]. This is believed to have been due to the edge-diffraction Green's function used in Howe's model, whereas the STE model is able to capture both constructive and destructive interferences, due to the different modes involved in the radiation integral, see Eq. (13).

3. Wavenumber-frequency spectra implementation

As discussed earlier, a prior knowledge of the boundary layer surface pressure fluctuations, in the form of wavenumber-frequency spectra, in the vicinity of the trailing edge is needed for the calculation of the far-field noise using the STE model. Even though the STE model is derived based on flat-plate assumptions, it is still applicable to airfoils operating in the fully attached flow regime, similar to Amiet's model, which has been successfully applied to airfoils at non-zero angles of attack, for instance by Roger et al. [44]. The underlying flat plate assumptions, such as frozen turbulence and linear scattering, hold at low to moderate angles of attack, depending on the specific flow conditions and airfoil geometry. For all test cases presented in this work, no flow separation was found and hence the STE model is applicable.

A major question remaining, however, is the wavenumber-frequency spectrum input needed for the STE noise prediction model. Prior research has shown that the boundary layer point spectrum can greatly change over the airfoil and serrations, particularly in the presence of a pressure gradient. The wavenumber-frequency model used for the modeling of the boundary layer and the location of extracting the boundary layer information is therefore of great importance. Various wavenumber-frequency models, such as the Corcos, Efimtsov, Smol'yakov and Tkachenko, Chase, TNO model, *etc.* have been developed and used in various applications [45]. In the absence of prior extensive near-field hydrodynamic information for serrated airfoils, here we will adopt two wavenumber-frequency models, namely Chase and TNO, to provide a comparative study. The Chase model has also been previously used by others [4,8], due to its simplicity. The TNO model provides a more physics-based prediction tool and has therefore been extensively used in engineering applications, particularly for wind turbine noise prediction [35,46]. To demonstrate the influence of the boundary layer information extraction location, a parametric study will also be performed in Section 4.2.

3.1. Chase wavenumber-frequency spectrum model

The Chase wavenumber-frequency spectrum model has been used extensively for various applications [37,40], including Howe's far-field trailing edge noise model [4]. The Chase wavenumber-frequency spectrum is given by

$$\Pi(\omega, k_1, k_2) = \frac{C_m \rho_0^2 v_*^3 k_1^2 \delta^5}{\left[(k_1 - \omega/U_c)^2 (\delta U_c v_*/3)^2 + \left(k_1^2 + k_2^2\right)\delta^2 + \chi^2\right]^{5/2}}. \tag{20}$$

Equation (12) requires the wavenumber-frequency spectrum to be integrated with respect to k_1 in order to calculate the far-field power spectral density, and hence, Eq. (20) is integrated over k_1 to obtain

$$\Pi(\omega, k_2) = \frac{4 C_m \rho_0^2 v_*^4 (\omega/U_c)^2 \delta^4}{U_c \left\{\left[(\omega/U_c)^2 + k_2^2\right]\delta^2 + \chi^2\right\}^2}. \tag{21}$$

The boundary layer thickness can be obtained using a panel method code such as XFoil [47] to avoid the need for a CFD

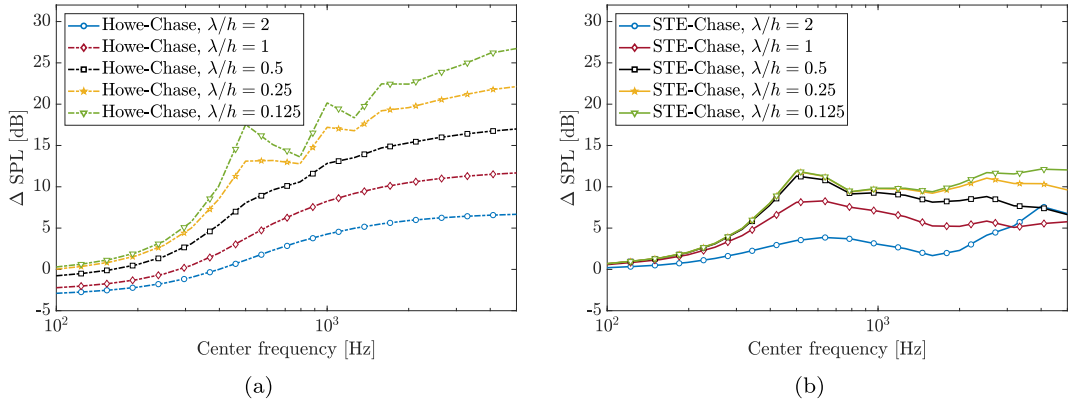

Fig. 3. Comparison of 1/3 octave band noise reduction between the STE and Howe's model for varying λ/h at a constant serration length of $h/c = 0.2$ for a $c = 0.2$ m NACA 0018 airfoil at $U_\infty = 30$ m/s: (a) Howe, (b) STE.

simulation, as used by Bertagnolio et al. [35] for instance. This would have the advantage of a very short run time. Alternatively, the boundary layer thickness can be acquired from experimental work or computational fluid dynamics (CFD) simulations of varying fidelity. In this study the boundary layer thickness is obtained from a RANS CFD simulation. The combination of the STE noise model, in conjunction with Chase wavenumber-frequency spectrum input, will be referred to as the "STE-Chase" method.

3.2. TNO wavenumber-frequency spectrum model

The second wavenumber-frequency spectrum model implemented as part of this work is the TNO model. The TNO model was originally devised by Parchen at the TNO Institute of Applied Physics [34]. It is computationally efficient, robust and models the physics of a turbulent boundary layer more accurately than most other models. Based on the TNO model, the wavenumber-frequency spectrum of a turbulent boundary layer can be found from Ref. [34],

$$\Pi(\omega, k_1, k_2) = 4\rho_0^2 \frac{k_1^2}{k_1^2 + k_2^2} \int_0^{\delta} \left(\Lambda_3 u_3^2 \left(\frac{\partial U_1}{\partial z_w} \right)^2 \Phi_{33} \Phi_m e^{-2|\mathbf{k}|z_w} \right) dz_w, \tag{22}$$

where z_w is the wall normal direction, Λ_3 is the vertical correlation length characterizing the vertical extent of the vertical turbulent velocity component (u_3), u_3^2 is the vertical Reynolds stress, $\frac{\partial U_1}{\partial z_w}$ is the velocity gradient in the wall normal direction through the boundary layer, Φ_{33} is the vertical velocity spectrum, Φ_m is the moving axis spectrum and $|\mathbf{k}|$ is the magnitude of the wavenumber vector. The vertical velocity spectrum has been defined as

$$\Phi_{33} = \frac{4}{9\pi k_e^2} \frac{k_1^2/k_e^2 + k_2^2/k_e^2}{\left[1 + (k_1/k_e)^2 + (k_2/k_e)^2\right]^{\frac{7}{3}}}, \tag{23}$$

where k_e describes the wavenumber of the energy containing eddies [35]. Similarly, the moving axis spectrum which describes how the turbulent velocity spectrum is distorted by the evolution of eddies as they are convected, is defined as follows [35],

$$\Phi_m = \frac{1}{\alpha_2 \sqrt{\pi}} e^{-\frac{(\omega - U_c k_1)^2}{\alpha_2^2}}, \tag{24}$$

where $\alpha_2 = 0.05 \frac{U_c}{\Lambda_3}$ and $U_c = 0.7 U_\infty$. As before, the STE far-field noise model, Eq. (12), requires the wavenumber-frequency spectrum to be integrated with respect to k_1, and hence, Eq. (22) is integrated over k_1 numerically. The boundary layer information necessary for the TNO wavenumber-frequency spectrum is obtained using RANS CFD. In what follows, the combination of the STE noise model and the TNO wavenumber-frequency spectrum input will be referred to as the "STE-TNO" approach.

In order to obtain the parameters required for the TNO wavenumber-frequency spectrum from a RANS CFD simulation, the approach of Bertagnolio et al. is adopted [48]. The boundary layer velocity profile and hence the boundary layer thickness can be obtained directly from the CFD simulation. In order to estimate the vertical Reynolds stress, the following relationship with the turbulent kinetic energy (TKE), k, obtained from the CFD simulation, can be used.

$$u_3^2 = \alpha_k k, \tag{25}$$

where α_k is taken as 0.30 and 0.45 for the pressure and the suction side, respectively [48]. The wavenumber of the energy containing eddies is related to the turbulent dissipation rate, ε, and the turbulent kinetic energy, k, by

$$k_e = 1.923 \frac{\varepsilon}{k^{3/2}}, \tag{26}$$

which in turn can be related to the vertical correlation length as follows,

$$\Lambda_3 = 0.747/k_e. \tag{27}$$

Lastly, the turbulence dissipation rate can be calculated from the specific turbulence dissipation rate $\overline{\omega}$, obtained from the RANS CFD simulation, as follows [49],

$$\varepsilon = 0.09 k \overline{\omega}. \tag{28}$$

It is important to note that the quantities required as input into the TNO model can be obtained from any RANS CFD simulation, both from airfoils with a straight trailing edge as well as from airfoils with a serrated trailing edge. Clearly though, a straight trailing edge simulation will not take the changes due to the presence of any serrations into account, and hence, the necessity to perform a CFD simulation of an airfoil with a serrated trailing edge will be investigated in Section 4.2.

3.3. Computational setup

A three-dimensional steady RANS CFD simulation is employed to study the NACA 0018 airfoil with and without a serrated trailing edge and to provide the necessary boundary layer information for use in Eqs. (21) and (22). The RANS equations were numerically solved using OpenFOAM, employing the $k-\overline{\omega}$ SST turbulence model [49]. The simulations were carried out for two effective angles of attack, $\alpha = 0^\circ$ and 6.6°, and the free stream velocities of $U_\infty = 30$ m/s and 40 m/s, corresponding to the chord-based Reynolds numbers of $3.9 \cdot 10^5$ and $5.2 \cdot 10^5$, respectively. Since the noise reduction prediction will be compared against the data from Leon et al. [14], the geometry of the airfoil and the serration follows their experimental setup and hence, the airfoil has a chord length of $c = 0.2$ m, with the trailing edge serrations having a wavelength of $\lambda = 20$ mm and amplitude of $h = 20$ mm, as shown in Fig. 4. A step trip with a height of 0.8 mm and a length of 2 mm was placed on both the suction and pressure sides of the airfoil at $x/c = 0.2$ to ensure a turbulent boundary layer over the trailing edge area of the airfoil. The computational domain for the simulation extends $20c$ in the streamwise direction, $10c$ in the normal direction and $0.4c$ in the spanwise direction, equivalent to four serration wavelengths, as illustrated in Fig. 4. At the airfoil surface, a non-slip boundary condition was applied, while a periodic boundary condition was used at the spanwise boundaries. A mesh convergence study has been performed before settling with approximately 3.7 million mesh elements and a y^+ value of 30 with wall functions. The mesh was generated using the snappyHex technique available within OpenFOAM. The geometry of the NACA 0018 airfoil as well as the boundary conditions can be seen in Fig. 4 and close-up views of the step trip and serration mesh are shown in Fig. 5.

Fig. 6 shows the pressure distribution for the NACA 0018 airfoil with straight trailing edge, as well as the pressure distribution in the root and tip planes for the serrated airfoil case, obtained from the RANS simulation. The pressure distribution results for the

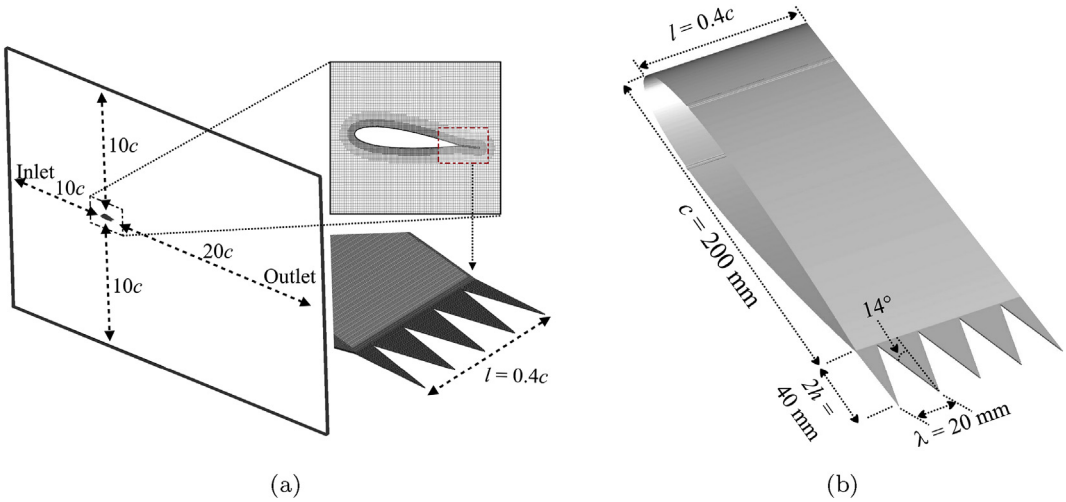

Fig. 4. (a) CFD domain and mesh overview and (b) NACA 0018 geometry.

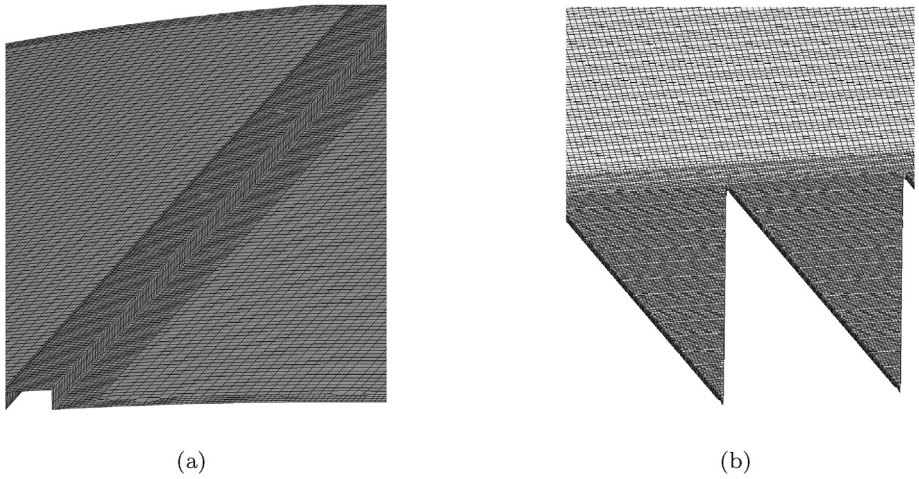

Fig. 5. Close-up views of (a) step trip surface mesh and (b) serration surface mesh.

baseline NACA 0018 airfoil, *i.e.* straight trailing edge, using XFoil is also provided for comparison. It can be seen in Fig. 4 that the pressure distribution does not change greatly between the straight and serrated case for $U_\infty = 30$ m/s at $\alpha = 0^\circ$ angle of attack. The CFD simulations show a strong pressure change around the step trip which was also observed in previous similar CFD simulations [50]. In the case of a NACA 0018 at $\alpha = 6.6^\circ$ and a free stream velocity of $U_\infty = 40$ m/s, both the suction side and pressure side exhibit a strong pressure change around the step trip again. There is also a slight difference in the suction peak when comparing the straight trailing edge baseline case to the serration pressure distribution. Additionally, the pressure distribution for the tip plane reveals a pressure difference over the serration leading to a small amount of additional lift in comparison to the baseline case.

4. Results and discussion

In this section, we will use the two far-field noise prediction tools, namely the STE and Howe's model, using different types of wavenumber-frequency spectra input, and will compare the results against available experimental data. The experimental data are taken from a recent work by Leon et al. [14], for a NACA 0018 airfoil with a chord length of 20 cm, span of 40 cm and flow velocities of $U_\infty = 30$ m/s, 35 m/s and 40 m/s. The airfoil is tripped at 20% chord using carborundum and the acoustic measurements were obtained using a beamforming microphone array consisting of 64 electret-condenser microphones located at a distance of 1.05 m from the airfoil. The sawtooth serrations used have a length of $2h = 4$ cm and a wavelength of $\lambda = 2$ cm. Two test cases are considered in the present work, firstly for a free stream velocity of $U_\infty = 30$ m/s and $\alpha = 0^\circ$ angle of attack and secondly for a free stream velocity of $U_\infty = 40$ m/s at an effective angle of attack of $\alpha = 6.6^\circ$ (corresponding to the geometric angle of attack of 12° [14]).

Firstly, the STE-Chase approach will be compared against the STE-TNO approach, where the CFD results were obtained from a straight trailing edge to ensure a consistent comparison. Secondly, CFD simulation results for the NACA 0018 airfoil with a serrated trailing edge will be used as an input into the STE-TNO approach. Since it is unclear which location on the serration should be chosen to extract the required boundary layer parameters as input in the STE model, a selection of several boundary layer extraction locations will be investigated to determine the sensitivity of the results with respect to the predicted far-field noise reduction. This will also permit a first comment on whether it is necessary to perform a CFD simulation with a serrated trailing edge or not.

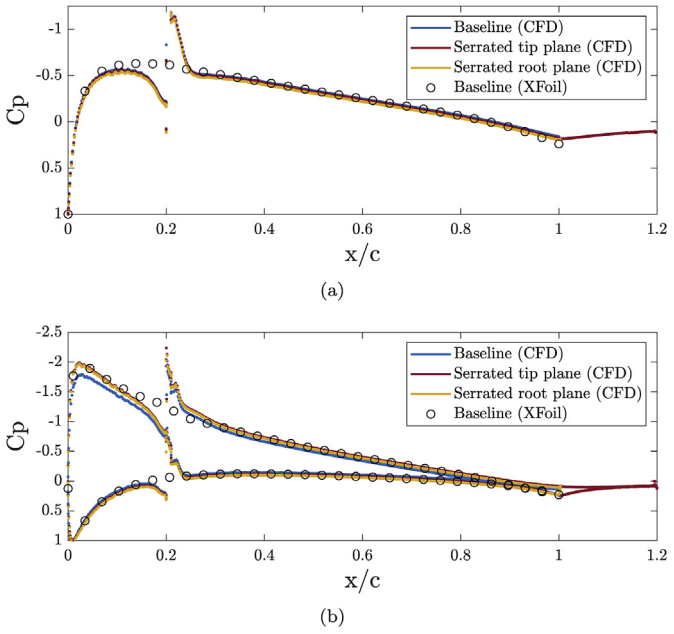

Fig. 6. Pressure distribution for the NACA 0018 airfoil with straight and serrated trailing edge: (a) $U_\infty = 30$ m/s at $\alpha = 0°$, (b) $U_\infty = 40$ m/s at $\alpha = 6.6°$.

4.1. Far-field prediction based on straight trailing edge CFD input

This section presents the predicted noise reduction (Δ *SPL*) results based on the CFD simulation for the NACA 0018 airfoil with a straight trailing edge. All required flow-field information has been extracted at $x/c = 0.99$. Fig. 7(a) and (b) present a comparison between the experimental noise reduction in 1/3 octave bands from Ref. [14], the noise reduction obtained using Howe's model, Eq. (16), as well as the noise reduction from the STE-Chase, Eqs. (12) and (21), and STE-TNO, Eqs. (12) and (22), models for both test cases. A positive Δ *SPL* value is indicative of a reduction in airfoil trailing edge noise. As can be seen from the results, Howe's noise reduction prediction increases for increasing frequencies, whilst the STE based models predict a peak noise reduction at around 630 Hz. Despite no available experimental data for low-frequencies, it can be seen for both test cases that for frequencies of up to 3 kHz the STE-Chase approach was able to predict the noise reduction more accurately, while the STE-TNO approach underpredicts the noise reduction. At high-frequencies (>3 kHz), the discrepancies between both STE-based models and the experimental measurements increase. The high-frequency deviation could be due to a number of reasons. For example, this can be due to the fact that the wavenumber-frequency spectra become less accurate at high-frequencies, in particular, the spanwise correlation length might decay more quickly than anticipated in the wavenumber-frequency spectra [20]. The discrepancy at higher frequencies may also not result from the STE model. Whilst theoretically, the noise at high-frequencies should also be reduced, previous experiments have shown that the high-frequency noise increase can be attributed to the serration valley flow, which cannot be captured by a scattering model [42]. The valley flow noise could possibly be captured using a high-fidelity CAA approach, which takes the flow field as input for the noise prediction, albeit with the associated high computational cost. However, the approach taken in this study, fundamentally based on Amiet's scattering model, is computationally much more attainable and therefore useful at a design stage. Additionally, the high-frequency deviation is unlikely to be of major concern for some practical applications due to the lower absolute noise levels of

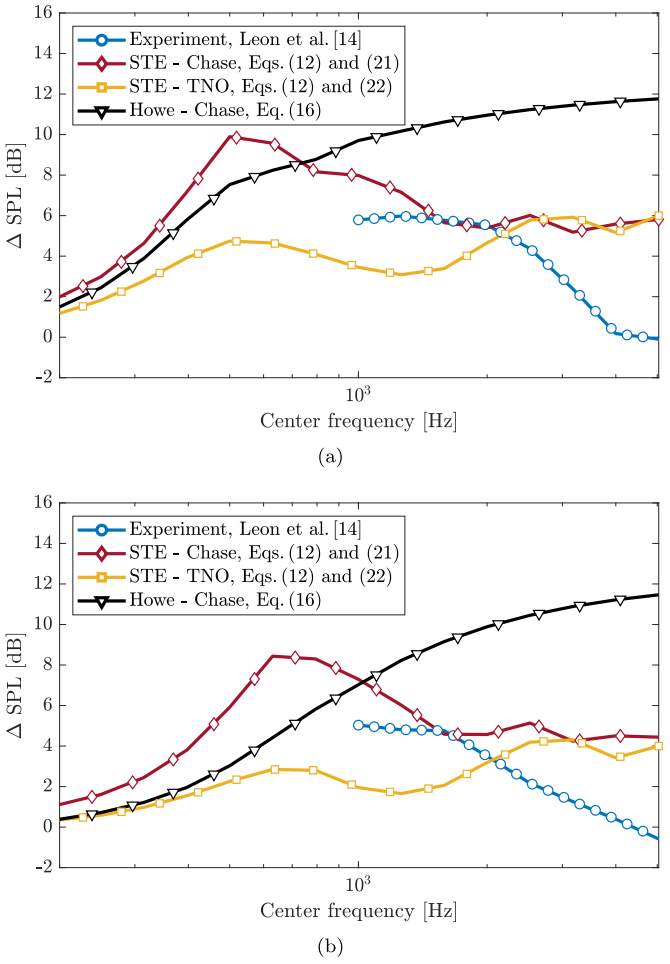

Fig. 7. 1/3 octave band noise reduction for a NACA 0018 airfoil with $\lambda = 2$ cm and $h = 2$ cm; experimental data from Ref. [14]: (a) $U_\infty = 30$ m/s at $\alpha = 0°$, (b) $U_\infty = 40$ m/s at $\alpha = 6.6°$.

trailing edge noise at high frequencies.

In contrast to the STE-based approaches, Howe's model over-predicts the noise reduction, as also observed in previous studies [42]. Howe's model additionally predicts increasing noise reductions for increasing frequencies in contrast to both STE-based predictions and the presented experimental data. Comparing the $\alpha = 0°$ case with the $\alpha = 6.6°$ case, it can be seen that both approaches capture the trend that the sound reduction potential is decreased at increased angles of attack, and thereby follows the experimental trend. The peak far-field noise reduction for the STE-Chase approach reduces from 10 dB at $\alpha = 0°$ to 8 dB at $\alpha = 6.6°$, whilst the peak far-field noise reduction for the STE-TNO approach reduces from 6 dB at $\alpha = 0°$ to 4 dB at $\alpha = 6.6°$.

4.2. Far-field prediction based on serrated trailing edge CFD input

This section utilizes the CFD simulation with a serrated trailing edge in order to investigate the changes to the predicted noise reduction due to the presence of a serration as well as its sensitivity to the boundary layer extraction location over the serration area using the STE-TNO approach. In contrast to the STE-TNO approach, the sound reduction prediction based on the STE-Chase approach would not vary much for the different boundary layer extraction location, because the boundary layer thickness, which is the only flow field input required for the STE-Chase approach, does not

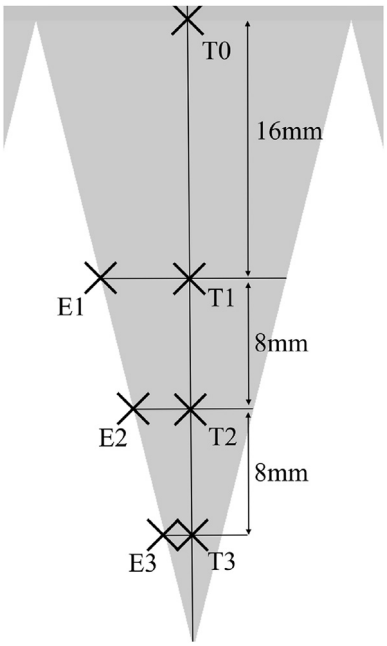

Fig. 8. Boundary layer extraction locations and naming convention.

change considerably as a result of the presence of the serrations, as will be seen in Fig. 9. As a result of the parametric study for the STE-TNO approach, one can therefore establish whether it is sufficient to perform a CFD analysis of an un-serrated airfoil or if the boundary layer information must be taken at a specific location over the serration. This is key in order to obtain the correct input for the STE model.

The parametric study with respect to the extraction location over the serration area is conducted for the locations displayed in Fig. 8, where "E" and "T" represent the edge-line of the serration and the tip-plane, respectively.

It is crucial to determine which location provides the best input into the STE-TNO model, as the TNO wavenumber-frequency spectrum is sensitive to changes in the boundary layer profile, vertical Reynolds stress changes and vertical correlation length. These parameters are influenced by the flow field changes due to the formation of the horseshoe vortices at the edges of the serration [9,16], and will therefore impact the noise reduction prediction. The changes to the flow field can clearly be seen in Fig. 9(a) and (b) depicting the velocity, turbulent kinetic energy (TKE) and turbulent dissipation boundary layer profiles for the suction side of the NACA 0018 airfoil at a free stream velocity of $U_\infty = 30$ m/s and $\alpha = 0°$, as well as $U_\infty = 40$ m/s and $\alpha = 6.6°$. It should be noted that the "baseline T0" case, represents the "T0" location without the serration being present, *i.e.* a straight trailing edge.

At $\alpha = 0°$, one can see in Fig. 9a that the boundary layer velocity profiles over the serration have a fuller profile, *i.e.* a reduced velocity deficit, when compared to the "T0" location. For a constant chordwise (x/c) position, the velocity profile is slightly fuller for the edge location ("E") when compared to the mid-plane location ("T") of the serration. Similarly, it can be seen that for the locations closer to the serration tip, the boundary layer velocity profiles become fuller, which matches the observations of Avallone et al. obtained using the Lattice Boltzmann method [20]. Similar observations can be made for the TKE energy and turbulent dissipation. For the locations closer to the tip of the serration, lower TKE as well as lower turbulent dissipation rates are observed. Equally, the presented results indicate that for a constant chordwise (x/c) position the TKE has decreased near the serration surface, whilst the turbulent dissipation has increased near the surface for the serration edge locations ("E") compared to the serration midplane locations ("T").

In the case of $\alpha = 6.6°$, Fig. 9b shows that the boundary layer velocity profiles have a reduced velocity deficit for the chordwise locations closer to the serration tip. For a constant chordwise (x/c) position, the velocity profile is again fuller for the midplane locations ("T") when compared to the edge locations ("E") of the serration. The turbulent dissipation is reduced toward the serration tip and the reduction is greater than that of $\alpha = 0°$, while for a constant chordwise (x/c) location, the edge locations ("E") display a higher level of dissipation. Lastly, it can be seen that TKE is again reduced toward the serration tip and that the TKE reduction for the serration edge locations ("E") compared to the serration midplane locations ("T") is significantly more pronounced than at $\alpha = 0°$. These results are consistent with the previous experimental observations by Liu et al. [16], which have found an increased flow mixing for flows passing over airfoil serrations due to the aforementioned horseshoe vortices on the serration edges, leading to fuller velocity boundary layer profiles and lower velocity fluctuations and thereby lower TKE.

Further insight into the flow field changes can be obtained by studying the contour plots of the wake turbulent kinetic energy. Fig. 10 shows the TKE contour plots at different wake locations, $x/c = 1.0$, 1.12 and 1.2, for the airfoil at $\alpha = 0°$ and $6.6°$. The results show that the TKE for the unserrated baseline case is uniform along the span at the chordwise location $x/c = 1.0$ for both angles of attack. The TKE results in Fig. 10c and d show the results for the serrated airfoil at a chordwise location of $x/c = 1.12$ for both the angles of attack. It is evident that reduced TKE levels can be seen between the serrations for both cases. At $\alpha = 0°$, the TKE on the suction and pressure side of the serration peaks in the midplane of the serration and reduces toward the serration edges and the area in between the neighboring serrations. At $\alpha = 6.6°$, an increased TKE is observed on the pressure side in comparison to the suction side. At the chordwise location of $x/c = 1.20$, *i.e.* at the very trailing edge of the serration the flow follows the same trend as that of location $x/c = 1.12$ for $\alpha = 0°$, but for $\alpha = 6.6°$ increased TKE levels can be found in the serration valley region, revealing an upward flow direction from the pressure side to the suction side, consistent with the experimental observations by Liu et al. [16].

Finally, Fig. 11(a) and (b) illustrate the predicted noise reduction in 1/3 octave bands for the various extraction locations, as well as the experimental data for both test cases of the NACA 0018 airfoil, *i.e.* $U_\infty = 30$ m/s at $\alpha = 0°$ and $U_\infty = 40$ m/s at $\alpha = 6.6°$ using the STE-TNO approach. Again, a positive Δ *SPL* value is indicative of a reduction in airfoil trailing edge noise. The baseline T0 case, represents the T0 location without the serration being present, *i.e.* with a straight trailing edge. It can be seen that at the peak experimental noise reduction, the agreement between the experimental data and the simulation improves as the boundary layer extraction location moves toward the serration tip. Significant differences between the "T0" location and the "E3" location of almost 5 dB have been found for both angles of attack. Additionally, it is clear that for the same chordwise (x/c) position, the edge location ("E") results in a higher noise reduction prediction compared to the serration midplane ("T"). These results are consistent with the earlier observation regarding the flow field changes over the serrations. The discrepancies at higher frequencies ($> 2–3$ kHz) are again present and the likely reasons have been elaborated in Section 4.1.

At $\alpha = 0°$, the "T0" and "baseline T0" (straight trailing edge) results are almost identical, revealing that the presence of the serration does not alter the flow field significantly before the

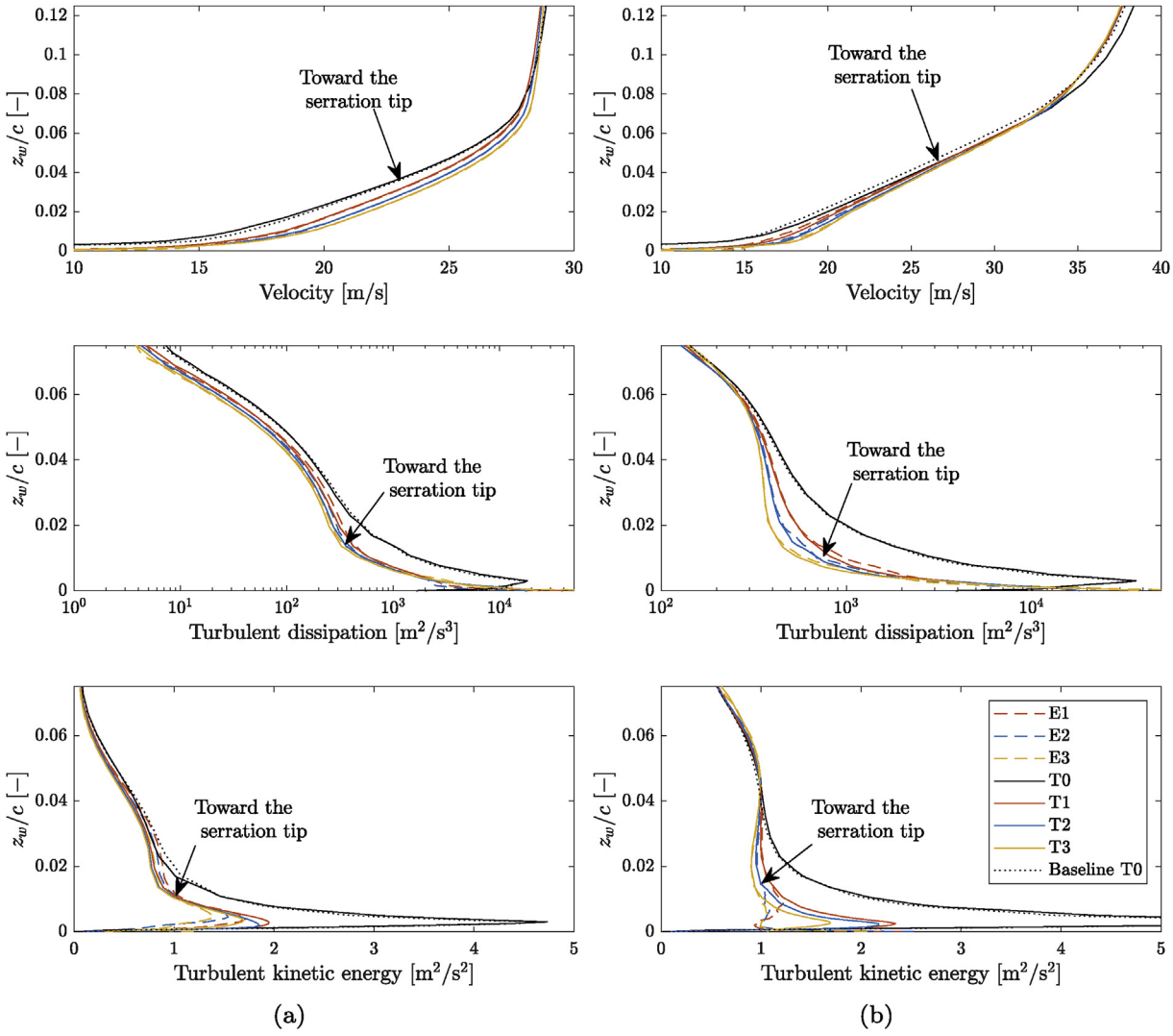

Fig. 9. Velocity, turbulent kinetic energy and turbulent dissipation boundary layer profiles in the wall-normal direction, z_w, for the suction side at different locations of a NACA0018 airfoil: (a/left column) $U_\infty = 30$ m/s at $\alpha = 0°$, (b/right column) $U_\infty = 40$ m/s at $\alpha = 6.6°$.

physical serration for symmetric airfoils at $\alpha = 0°$. However, at $\alpha = 6.6°$, there is a noticeable difference between the "T0" and "baseline T0" location, because of the induced upward flow motion due to the pressure difference between the suction and pressure sides of the airfoil. Similar to the results from Section 4.1, it is also clear from Fig. 11(a) and (b) that for the STE-TNO approach, an increased angle of attack leads to a smaller noise reduction.

The strong variation of the predicted Δ *SPL* depending on the boundary layer extraction location for the STE-TNO approach, demonstrated the fact that a prior knowledge of the wavenumber-frequency spectrum plays an important role for the accurate prediction of noise from serrated airfoils. This is in agreement with the flow field changes resulting from the presence of the serrations, which have revealed a strongly varying flow field over the serrations. Horseshoe vortices have been shown to develop over the edges of each serration, in both experiment and simulation [9,14,16,17,21]. Gruber [42] and Ragni et al. [18] have shown that the surface pressure fluctuations change rapidly over a serration, and investigations by Avallone et al. [20,21] have revealed noticeable changes in the velocity fluctuations in the boundary layer over serrations. It can, therefore, be concluded that serrations clearly impact the local flow-field, and therefore the sound radiation. The results presented in this paper show a sensitivity of the STE scattering model toward the utilized wavenumber-frequency model and the boundary layer extraction location. The need to further investigate the changes to the wavenumber-frequency spectrum due to the presence of a serrated trailing edge is therefore demonstrated.

5. Conclusions

A novel trailing edge noise reduction prediction model developed by Lyu et al. for serrated airfoils has been implemented and validated successfully for straight and serrated trailing edges for realistic airfoils. The implementation of the serration model is computationally efficient and consequently, it would also be feasible to use this code to optimize serration geometries within a larger optimization framework. The necessary boundary layer input parameters are obtained from RANS CFD simulations. Two wavenumber-frequency spectra, namely Chase model and the TNO model, are implemented in the model, which is shown to provide a better sound reduction prediction compared to Howe's model. This is believed to be due to the fact that the iterative solution provides a more accurate modeling to the scattering response than the Green's

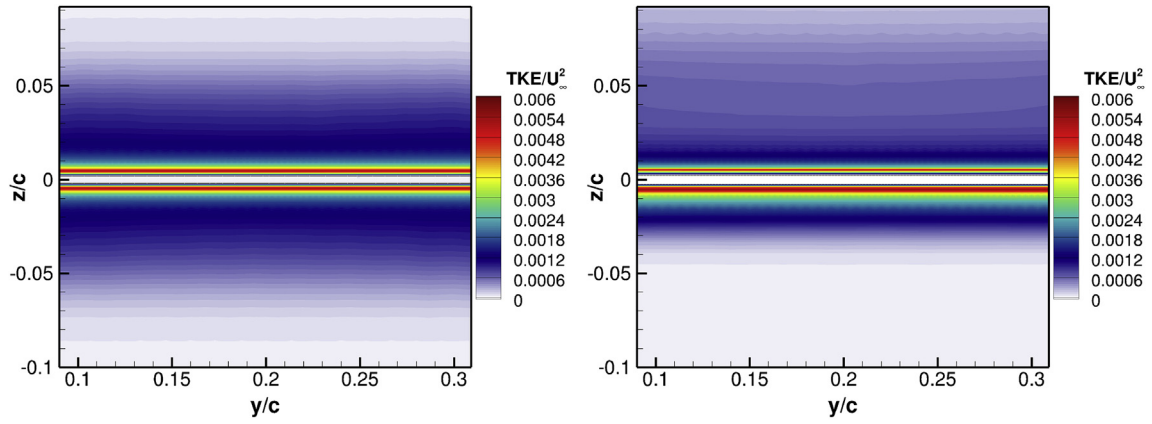

(a) x/c = 1.0, baseline, $\alpha = 0°$.

(b) x/c = 1.0, baseline, $\alpha = 6.6°$.

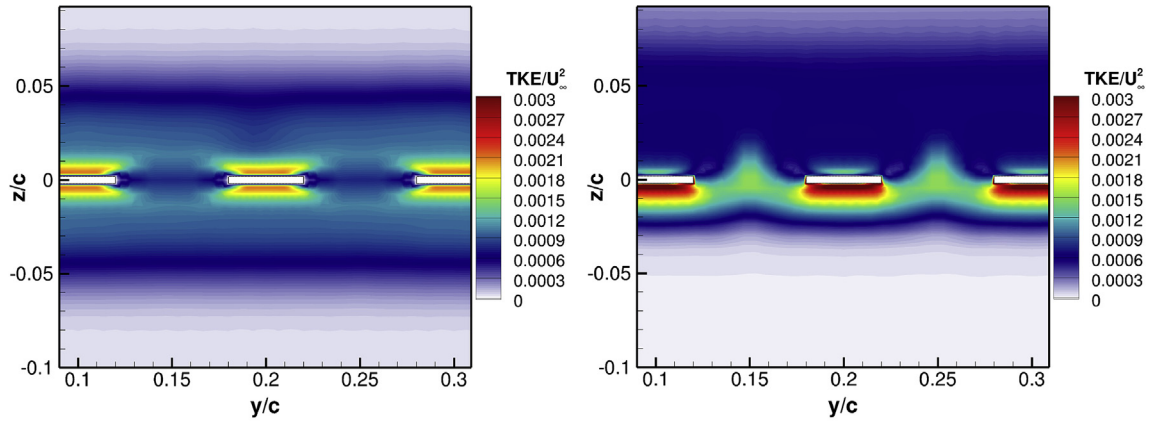

(c) x/c = 1.12, serrated airfoil, $\alpha = 0°$.

(d) x/c = 1.12, serrated airfoil, $\alpha = 6.6°$.

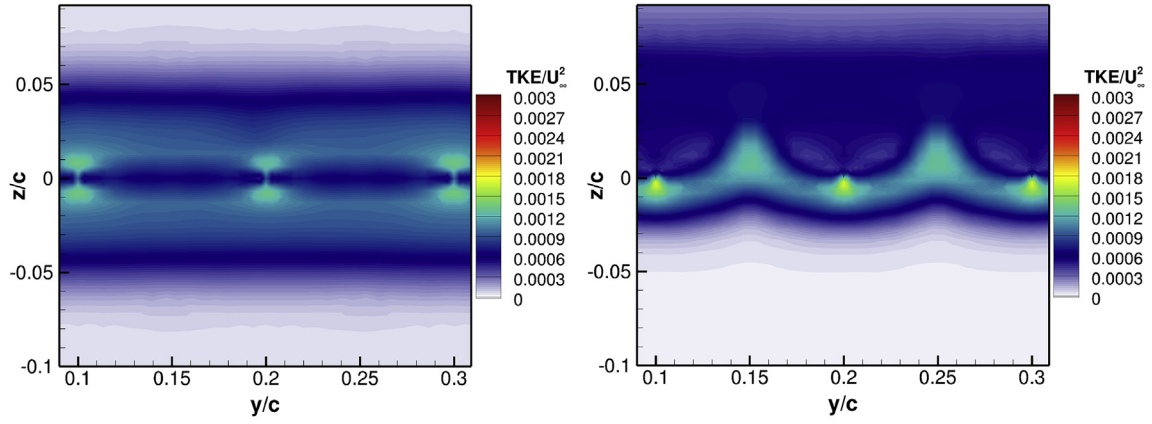

(e) x/c = 1.2, serrated airfoil, $\alpha = 0°$.

(f) x/c = 1.2, serrated airfoil, $\alpha = 6.6°$.

Fig. 10. The contours of Turbulent kinetic energy at various chordwise location for the baseline and serrated airfoil at angles of attack $\alpha = 0°$ and 6.6°.

function used by Howe. Additionally, the proposed model allows higher Mach number flows to be considered as the solution satisfies the convective wave equation.

Comparing the Chase-based and TNO-based boundary layer inputs, it is clear that Chase's spectrum does not rely on a full CFD simulation and can therefore be more efficient to compute. However, assuming an appropriate boundary layer extraction location, the authors hypothesize that the TNO-based boundary layer approach will result in more robust and reliable predictions, as it takes the flow field changes into account which are caused as a result of the flow and serration interaction. Additionally, it has been shown that different boundary layer extraction locations over the serration can greatly influence the predicted sound reduction, by up to 5 dB, TNO-based approach. In order to further assess the capabilities of the proposed prediction method, a more comprehensive study with different airfoils would be required. It would also be

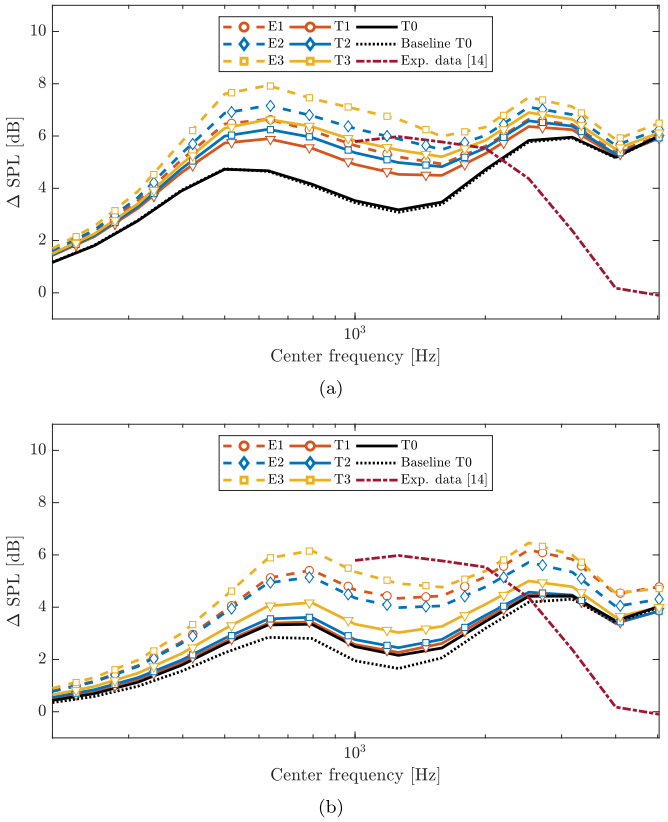

Fig. 11. 1/3 octave band noise reduction for various boundary layer extraction locations for a NACA0018, STE-TNO approach, Eqs. (12) and (22): (a) $U_\infty = 30$ m/s at $\alpha = 0°$, (b) $U_\infty = 40$ m/s at $\alpha = 6.6°$.

advantageous to experimentally or numerically investigate the changes to the wavenumber-frequency spectra caused by the presence of serrations. Further experimental and theoretical investigations are planned to firstly improve our understanding of trailing edge noise reduction using serrations and also secondly further improve our prediction capabilities.

Declaration of interest

None.

References

[1] L.D. Knopper, C.A. Ollson, Health effects and wind turbines: a review of the literature, Environ. Health 10 (1) (2011) 78–88, https://doi.org/10.1186/1476-069X-10-78.
[2] P. Venugopal, L. Cheung, G. Jothiprasad, S.K. Lele, Large eddy simulation of a wind turbine airfoil at high angle of attack, in: Center for Turbulence Research, Proceedings of the Summer Program 2012, Stanford, California, United States, 2012, pp. 157–165.
[3] T.F. Brooks, D.S. Pope, M.A. Marcolini, Airfoil Self-Noise and Prediction, Tech. Rep., NASA Langley Research Center, Hampton, Virginia, United States, 1989, https://doi.org/10.1111/j. 1469-7580.2012.01504.x.
[4] M.S. Howe, Aerodynamic noise of a serrated trailing edge, J. Fluids Struct. 5 (1991) 33–45, https://doi.org/10.1016/0889-9746(91)80010-B.
[5] S.A.S. Ali, M. Azarpeyvand, C.R.I. Da Silva, Trailing-edge flow and noise control using porous treatments, J. Fluid Mech. 850 (2018) 83–119, https://doi.org/10.1017/jfm.2018.430.
[6] A. Afshari, M. Azarpeyvand, A.A. Dehghan, M. Szoke, Effects of streamwise surface treatments on trailing edge, in: 23rd AIAA/CEAS Aeroacoustics Conference, AIAA 2017-3499, Denver, Colorado, United States, 2017, https://doi.org/10.2514/6.2017-3499.
[7] I.A. Clark, D. Baker, W.N. Alexander, W.J. Devenport, S.A. Glegg, J. Jaworski, N. Peake, Experimental and theoretical analysis of bio-inspired trailing edge noise control devices, in: 22nd AIAA/CEAS Aeroacoustics Conference, AIAA 2016-3020, Lyon, France, 2016, https://doi.org/10.2514/6.2016-3020.
[8] M. Azarpeyvand, M. Gruber, P.F. Joseph, U. Kingdom, an analytical investigation of trailing edge noise reduction using novel serrations, in: 19th AIAA/CEAS Aeroacoustics Conference, Berlin, Germany, 2013, https://doi.org/10.2514/6.2013-2009.
[9] D. Ragni, F. Avallone, W.C.P. van der Velden, Concave serrations on broadband trailing edge noise reduction, in: 23rd AIAA/CEAS Aeroacoustics Conference, AIAA 2017-4174, Denver, Colorado, United States, 2017, https://doi.org/10.2514/6.2017-4174.
[10] F. Avallone, W.C.P. van der Velden, D. Ragni, Benefits of curved serrations on broadband trailing-edge noise reduction, J. Sound Vib. 400 (2017) 167–177, https://doi.org/10.1016/j. jsv.2017.04.007.
[11] T. Dassen, R. Parchen, J. Bruggeman, F. Hagg, Results of a wind tunnel study on the reduction of airfoil self-noise by the application of serrated blade trailing edges, in: 1996 European Union Wind Energy Conference and Exhibition, Gothenburg, Sweden, 1996.
[12] D.J. Moreau, C.J. Doolan, Noise-reduction mechanism of a flat-plate serrated trailing edge, AIAA J. 51 (2013), https://doi.org/10.2514/1.J052436.
[13] M. Gruber, M. Azarpeyvand, P.F. Joseph, Airfoil trailing edge noise reduction by the introduction of sawtooth and slitted trailing edge geometries, in: Proceedings of 20th International Congress on Acoustics, ICA, vol. 10, 2010, pp. 1–9.
[14] C. Arce Leon, F. Avallone, D. Ragni, S. Pröbsting, PIV investigation of the flow past solid and slitted sawtooth serrated trailing edges, in: 54th AIAA Aerospace Sciences Meeting, AIAA SciTech Forum, AIAA 2016-1014, San Diego, California, United States, 2016, https://doi.org/10.2514/6.2016-1014.
[15] S. Oerlemans, M. Fischer, T. Maeder, Klaus Kögler, Reduction of wind turbine noise using optimized airfoils and trailing-edge serrations, AIAA J. 47 (6) (2009) 1470–1481, https://doi.org/10.2514/1.38888.
[16] X. Liu, H.K. Jawahar, M. Azarpeyvand, R. Theunissen, Aerodynamic performance and wake development of airfoils with serrated trailing-edges, AIAA J. 47 (2009) 1470–1481, https://doi.org/10.2514/1. 38888.
[17] T.P. Chong, A. Vathylakis, On the aeroacoustic and flow structures developed on a flat plate with a serrated sawtooth trailing edge, J. Sound Vib. 354 (2015) 65–90, https://doi.org/10.1016/j.jsv.2015.05.019.
[18] D. Ragni, F. Avallone, W.C.P. van der Velden, D. Casalino, Measurements of near-wall pressure fluctuations for trailing-edge serrations and slits, Exp. Fluid 60 (2019), https://doi.org/10.1007/s00348-018-2654-5.
[19] M.P.J. Sanders, L.D. de Santana, M. Azarpeyvand, C.H. Venner, Unsteady surface pressure measurements on trailing edge serrations based on digital MEMS microphones, in: 2018 AIAA/CEAS Aeroacoustics Conference, AIAA 2018-3290, Atlanta, Georgia, United States, 2018, https://doi.org/10.2514/6.2018-3290.
[20] F. Avallone, W.C.P. van der Velden, D. Ragni, D. Casalino, Noise reduction mechanisms of sawtooth and combed-sawtooth trailing-edge serrations, J. Fluid Mech. 848 (2018) 560–591, https://doi.org/10.1017/jfm.2018.377.
[21] F. Avallone, S. Pröbsting, D. Ragni, Three-dimensional flow field over a trailing-edge serration and implications on broadband noise, Phys. Fluids 28 (2016), https://doi.org/10.1063/1.4966633.
[22] R.D. Sandberg, L.E. Jones, Direct numerical simulations of low Reynolds number flow over airfoils with trailing-edge serrations, J. Sound Vib. 330 (2011) 3818–3831, https://doi.org/10.1016/j.jsv.2011.02.005.
[23] W.R. Wolf, S.K. Lele, Trailing-edge noise predictions using compressible large-eddy simulation and acoustic analogy, AIAA J. 50 (2012) 2423–2434, https://doi.org/10.2514/1.J051638.
[24] R.D. Sandberg, N.D. Sandham, Direct numerical simulation of turbulent flow past a trailing edge and the associated noise generation, J. Fluid Mech. 596 (2008) 353–385, https://doi.org/10.1017/S0022112007009561.
[25] C. Bogey, C. Bailly, D. Juve, Computation of flow noise using source terms in Linearized Euler's equations, AIAA J. 40 (2002) 235–243, https://doi.org/10.2514/2.1665.
[26] H.K. Jawahar, Y. Lin, M. Savill, Large eddy simulation of airfoil self-noise using OpenFOAM, Aircraft Eng. Aero. Technol. 90 (2018) 126–133, https://doi.org/10.1108/AEAT-05-2015-0130.
[27] H.K. Jawahar, Q. Ai, M. Azarpeyvand, Experimental and numerical investigation of aerodynamic performance of airfoils fitted with morphing trailing-edges, in: 23rd AIAA/CEAS Aeroacoustics Conference, AIAA 2017-3371, Denver, Colorado, United States, 2017, https://doi.org/10.2514/6.2017-3371.
[28] J.E. Ffowcs Williams, D.L. Hawkings, Sound generation by turbulence and surfaces in arbitrary motion, Phil. Trans. Math. Phys. Eng. Sci. 264 (1969) 321–342, https://doi.org/10.1098/rsta.1969.0031.
[29] M.C. Jacob, J. Boudet, D. Casalino, M. Michard, A rod-airfoil experiment as benchmark for broadband noise modeling, Theor. Comput. Fluid Dynam. 19 (2005) 171–196, https://doi.org/10.1007/s00162-004-0108-6.
[30] E. Liu, S. Yan, S. Peng, L. Huang, Y. Jiang, Noise silencing technology for manifold flow noise based on ANSYS fluent, J. Nat. Gas Sci. Eng. 29 (2016) 322–328, https://doi.org/10.1016/j.jngse.2016.01.021.
[31] J. Liu, N. Chu, S. Qin, D. Wu, Numerical simulations of bubble formation and acoustic characteristics from a submerged orifice: the effects of nozzle wall configurations, Chem. Eng. Res. Des. 123 (2017) 130–140, https://doi.org/10.1016/j.cherd.2017.05.002.
[32] R.K. Amiet, Acoustic radiation from an airfoil in a turbulent stream, J. Sound Vib. 41 (1975) 407–420, https://doi.org/10.1016/S0022-460X(75)80105-2.
[33] S. Moreau, M. Roger, Back-scattering correction and further extensions of Amiet's trailing-edge noise model. Part 1: Theory, J. Sound Vib. 286 (2005) 477–506, https://doi.org/10.1016/j jsv.2008.11.051.

[34] R.R. Parchen, Progress Report DRAW: A Prediction Scheme for Trailing Edge Noise Based on Detailed Boundary Layer Characteristics, TNO-Report HAG-RPT, TNO Institute of Applied Physics, 1998.
[35] F. Bertagnolio, Trailing Edge Noise Model Applied to Wind Turbine Airfoils, Risø-R-163, Risø National Laboratory, Technical University of Denmark, Roskilde, Denmark, 2008, ISBN 9788755036567.
[36] D.J. Moreau, L.A. Brooks, C.J. Doolan, Flat plate self-noise reduction at low-to-moderate Reynolds number with trailing edge serrations, in: Proceedings of Acoustics 2011, Gold Coast, Australia, 2011.
[37] B. Lyu, M. Azarpeyvand, S. Sinayoko, Prediction of noise from serrated trailing edges, J. Fluid Mech. 793 (2016) 556–588, https://doi.org/10.1017/jfm.2016.132.
[38] A. Fischer, F. Bertagnolio, W.Z. Shen, J. Madsen, Noise model for serrated trailing edges compared to wind tunnel measurements, J. Phys. Conf. Ser. 753 (2016), https://doi.org/10.1088/1742-6596/753/2/022053.
[39] X. Huang, Theoretical model of acoustic scattering from a flat plate with serrations, J. Fluid Mech. 819 (2017) 228–257, https://doi.org/10.1017/jfm.2017.176.
[40] L.J. Ayton, Analytic solution for aerodynamic noise generated by plates with spanwise-varying trailing edges, J. Fluid Mech. 849 (2018) 448–466, https://doi.org/10.1017/jfm.2018.431.
[41] R.K. Amiet, Noise due to turbulent flow past a trailing edge, J. Sound Vib. 47 (1976) 387–393, https://doi.org/10.1016/0022-460X(76)90948-2.
[42] M. Gruber, Airfoil Noise Reduction by Edge Treatments, Ph.D. thesis, University of Southampton, 2012.
[43] M.S. Howe, Noise produced by a sawtooth trailing edge, J. Acoust. Soc. Am. 90 (1991) 482–487.
[44] S. Moreau, M. Roger, Back-scattering correction and further extensions of Amiet's trailing-edge noise model. Part II: Application, J. Sound Vib. 323 (2009) 397–425, 10. 1016/j.jsv.2008.11.051.
[45] W.R. Graham, A comparison of models for the wavenumber-frequency spectrum of turbulent boundary layer pressures, J. Sound Vib. 206 (1997) 541–565, https://doi.org/10.1006/jsvi. 1997.1114.
[46] F. Bertagnolio, H.A. Madsen, C. Bak, Experimental validation of TNO trailing edge noise model and application to airfoil optimization, in: European Wind Energy Conference, Marseille, France, 2009.
[47] M. Drela, XFOIL: an analysis and design system for low Reynolds number airfoils, in: Low Reynolds Number Aerodynamics: Proceedings of the Conference Notre Dame, Notre Dame, Indiana, United States, 1989.
[48] F. Bertagnolio, A. Fischer, W. Jun Zhu, Tuning of turbulent boundary layer anisotropy for improved surface pressure and trailing-edge noise modeling, J. Sound Vib. 333 (2014) 991–1010, https://doi.org/10.1016/j.jsv.2013.10.008.
[49] F.R. Menter, M. Kuntz, R. Langtry, Ten years of industrial experience with the SST turbulence model, in: 4th International Symposium on Turbulence, Heat and Mass Transfer, 2003. Antalya, Turkey.
[50] J. Winkler, R.D. Sandberg, S. Moreau, Direct numerical simulation of the self-noise radiated by an airfoil in a narrow stream, in: 18th AIAA/CEAS Aeroacoustics Conference, AIAA 2012-2059, Colorado Springs, Colorado, United States, 2012, https://doi.org/10.2514/6.2012-2059.